Global surface cooling: the atmospheric fast feedback response to a collapse of the thermohaline circulation

Laurian, A., Drijfhout, S. S., Hazeleger, W., and van Dorland, R.

Corresponding author: Audine Laurian, KNMI, Royal Netherlands Meteorological Institute, De Bilt, The Netherlands, email: laurian@knmi.nl

Abstract

In the ECHAM5/MPI-OM model a collapse of the Atlantic thermohaline circulation results in a global surface cooling of 0.72 K. The mechanisms that are responsible for this cooling are investigated. Additional experiments were performed with a one-dimensional radiative convective model in which anomalies from the climate model were prescribed. Fast atmospheric feedbacks are essential to maintain and strengthen the global surface cooling caused by a THC collapse. Reduced downward long wave radiation exceeds the decreased upward long wave radiation. This decreased downward long wave radiation is caused by reduced water vapor content rather than by ice-albedo feedbacks. Also, the decrease in water vapor is much stronger than suggested by the water vapor feedback expected from the simulated albedo change. The large decrease in water vapor is the main feedback. On the regional scale, changes in cloud water and cloud radiative forcing further modify the surface cooling.

1. Introduction

Climate models show that a collapse of the Atlantic thermohaline circulation (THC) leads to a reduction in northward oceanic heat transport (OHT) and a strong cooling in the Northern Hemisphere, in particular in the North Atlantic Ocean (*Manabe and Stouffer*, 1994; *Vellinga and Wood*, 2002; *Stouffer et al.*, 2006). The reduced northward OHT in the Atlantic causes a dipole pattern in the surface temperature response with a slight warming in the Southern Hemisphere. Evidence of this dipole pattern has been found in paleodata, probably associated with a reduction of the THC (*Bond et al.*, 1992; *Blunier and Brook*, 2001). The atmospheric heat transport (AHT) increases to compensate for the decreased OHT but this compensation is far from complete at mid-high latitudes (*Cheng et al.*, 2007; *Vellinga et Wu*, 2008). Bjerknes compensation between OHT and AHT does not apply for this large fluctuation of the THC because the ocean heat content changes. A readjustment of the global energy budget occurs to account for the change in net meridional energy transport. Over a large part of the globe the top of the atmosphere (TOA) and surface flux anomalies resulting from the new equilibrium are of comparable magnitude, except in the North Atlantic where the anomalous surface cooling is strongest (*Vellinga and Wu*, 2008).

In this paper we investigate how a collapse of the THC can lead to a fast global surface cooling. The THC collapse was induced by freshwater hosing in the northern North Atlantic. We study the response of the surface energy budget, albedo, cloud cover and water vapor. Using a one-dimensional radiative convective model in which anomalies from the climate model were prescribed, sensitivity experiments were performed to assess the role of water vapor, ice/albedo feedback and cloud cover in causing the global surface cooling.

2. Models and experiments

2.1. Hosing experiments with the ECHAM5/MPI-OM climate model

The ECHAM5/MPI-OM climate model is described in *Roeckner et al.* (2003) and *Marsland et al.*

(2003). The ocean model has a horizontal resolution of about 1.4° by 1.4° away from the poles, it is highest near the poles (O(20-40 km)) and the meridional resolution is refined near the equator to 0.5°. It has 40 vertical levels. The atmospheric model has 31 vertical levels and a horizontal resolution of T63.

We use a five-member ensemble simulation out of a 17-member ensemble that was performed over the period 1950-2100 (*Sterl et al.*, 2008). From 1950 to 2000 the simulations were forced by the concentrations of greenhouse gases (GHG) and tropospheric sulfate aerosols specified from observations. From 2001 to 2100 the simulations followed the SRES A1b scenario (*Nakicenovic et al.*, 2000). Each simulation was initialized from a single long simulation in which historical GHG concentrations have been used until 1950. In an additional ensemble, a freshwater anomaly of 1 Sv (1 Sv= $10^6 m^3.s^{-1}$) was uniformly applied in the northern North Atlantic Ocean between 50°N and 70°N from 2001 onwards, starting from the five initial states of the first ensemble. Here we address the global surface cooling due to a THC collapse by comparing the ensemble means of the perturbed simulations (called HOSING) to the associated control simulations (called ENSMALL) over the period 2091-2100.

2.2. Sensitivity experiments using a radiative convective model

The role of water vapor and ice/albedo feedbacks in accounting for the global surface cooling was investigated using a one-dimensional radiative convective model (RCM). This RCM (*Van Dorland*, 1999) is based on original concepts of *Manabe and Strickler* (1964) and *Manabe and Wetherald* (1967). Clouds are specified at three levels representing low, middle and high clouds. The non-radiative fluxes (sensible and latent heat) are computed from the surface energy balance.

Sensitivity experiments were performed by adding anomalous water vapor, albedo and cloud cover due to a THC collapse to the equilibrium values in the RCM. In some experiments the relative humidity (RH) was kept fixed to study the effect of water vapor feedback on prescribed changes in albedo and cloud cover.

3. Global responses to a THC collapse

3.1. Two-meter air temperature response

The two-meter cooling pattern resulting from a THC collapse is shown in Fig. 1 (left panel). An interhemispheric dipole pattern is evident with strong cooling in the Northern Hemisphere and lesser warming in the Southern Hemisphere. Often this dipole pattern is explained by a reduction of northward OHT by the THC. Here we show that atmospheric processes play a crucial role in maintaining and strengthening the global surface cooling due to the THC collapse. The globally averaged cooling is 0.72 K which is consistent with the 1°C cooling found by *Stouffer et al.* (2006). The cooling is accomplished in twenty years (Fig. 1, right).

3.2. Surface radiation budget response

The radiation budget at the surface is:

$$\text{SW up} + \text{LW up} + \text{LH} + \text{SH} = \text{SW down} + \text{LW down}$$

where SW (LW) stands for short (long) wave radiation, LH (SH) stands for latent (sensible) heat, and up and down stand for upward and downward. These budget terms are shown for the ENSMALL and HOSING ensemble means (Fig.2, left) and for the difference between HOSING and ENSMALL (Fig.2, right).

The global decrease in LH (1.42 $W.m^{-2}$; Fig. 2, right) has a spatial pattern shown in Fig.3 (upper left). It is very similar to that of the evaporation response (not shown), suggesting the important role of the water vapor response for the surface radiation budget change. The upward LW radiation is set by the ocean-driven surface cooling via Stefan-Boltzmann's law (see Fig. 1, left). Its global decrease of

3.59 $W.m^{-2}$ is more than balanced by decreased downward LW radiation (4.03 $W.m^{-2}$; Fig. 2, right). The pattern of downward LW is rather similar to that of upward LW (Fig. 3, upper right), but it features no change over the Alps and a stronger increase over the Sahel (not shown). Because decreased upward LW is overcompensated by decreased downward LW, the LW response results in a net surface cooling. This net cooling is balanced by heating due to decreased LH. Both LH and LW responses are dominated by water vapor content.

The colder surface temperatures associated with a THC collapse in ECHAM5/MPI-OM lead to a 4.8% increase in albedo. This albedo response plays a role in the global surface cooling and in the surface energy budget response at high latitudes. The increased upward SW radiation (0.45 $W.m^{-2}$) is therefore strongest at high latitudes where ice cover and albedo increase (Fig. 3, lower left). The pattern of the downward SW response (0.36 $W.m^{-2}$ decrease) is associated with the change in cloud water (Fig. 3, lower right; Fig. 4, lower left). The net response in SW is small and unimportant.

The dominant terms in the surface energy budget are the decreased upward and downward LW radiation (Fig. 2, right). Both terms are related to ice/albedo, cloud cover, and water vapor responses. To disentangle these responses and assess their respective contribution to the global surface cooling, sensitivity experiments were performed using a one-dimensional radiative convective model.

4. Sensitivity experiments with the RCM

The sensitivity experiments are detailed in Table 1. The reference experiment has prescribed albedo, cloud cover and water vapor to reproduce the 20th century's climate. The prescribed water vapor anomaly (experiments q_NoFb, Alb-q_NoFb, and Cld-Alb-q_NoFb) is taken from the difference between the HOSING and ENSMALL ensembles interpolated on the RCM levels and added to the RCM reference profile. The prescribed albedo change (experiments Alb_NoFb, Alb_Fb, Alb-q_NoFb and Cld-Alb-q_NoFb) is taken to be consistent with the surface upward SW response to a THC collapse (2%

increased albedo, rather than the globally averaged increase in albedo of 4.8%). This difference is due to the fact that an albedo change in the tropics has a much larger effect on the surface radiation balance than a similar change in an equally large area near the poles, because the incoming solar radiation is much less near the poles. The prescribed cloud cover anomalies (experiments Cld_Fb and Cld-Alb-q_NoFb) are taken from the difference between HOSING and ENSMALL. The globally averaged cloud cover increases by 0.33%. One third of this anomaly was added to the low-level cloud cover and two-third to the mid-level cloud cover, consistent with the vertical profile in the climate model. Cloud water content was prescribed in a similar way, with a decrease of 0.003 $g.m^{-2}$ at mid-level and a decrease of 0.007 $g.m^{-2}$ at low-level. When the water vapor is prescribed and RH is free to adjust, no water vapor feedback is operational, and conversely. Table 1 also shows the anomalous surface temperature and water vapor content, computed as the difference between an experiment and the reference run.

The combined effects of decreased water vapor and increased albedo are necessary to account for a surface cooling of 0.62 K, close to the 0.72 K cooling due to a THC collapse (Table 1, Alb-q_NoFb). The effect of increased albedo alone, even with water vapor feedback switched on, is much too weak to account for the surface cooling (Alb_NoFb: -0.08 K and Alb_Fb: -0.15 K). On the other hand, the effect of decreased water vapor already explains the largest part of the net surface cooling (q_NoFb: -0.53 K). These results indicate that the reduced LW is a response to decreased water vapor and reduced GHG trapping, rather than a response to the increased albedo. This is further corroborated by the changes in surface specific humidity which correlate perfectly with the changes in surface temperature (Fig. 4, upper left). Note that the anomalous surface upward and downward LW and SW radiation related to the prescribed anomalies described in Table 1 are of the order of magnitude of those due to the THC collapse in the climate model (not shown). The increased cloud cover (and decreased liquid water content) results in a weak surface cooling of 0.01 K (Cld_Fb). The cloud response in the RCM does not play an important role in the global surface cooling (compare Alb-q_NoFb and Cld-Alb-q_NoFb). However, the vertical distribution is rudimentary in the RCM and only the net global effect of clouds can be assessed. Regional differences and nonlinearities associated with cloud feedbacks require further analysis of the climate model rather than the RCM.

In addition to the primary ocean-driven surface cooling, changes in cloud water and cloud radiative forcing (CRF) further modify the surface temperature response on the regional scale. The globally averaged CRF decreases by 0.04 $W.m^{-2}$ but it decreases by up to 30 $W.m^{-2}$ over the eastern North Atlantic, in association with an increase in cloud water (Fig. 4, lower panels). The increased surface RH (up to 6%; not shown) is temperature-driven (*Laurian et al.*, 2009). It is associated with enhanced surface cooling driven by the cloud response, via the Clausius-Clapeyron relation. Moist static energy (MSE) decreases in the Northern Hemisphere (Fig. 4, upper right). Drier and colder air is brought from western and northwestern Europe to Siberia, leading to reduced cloud cover (6%; not shown) and cloud water (Fig. 4, lower left) which act to cut the surface energy supply. Decreased soil wetness and associated increased snow cover (not shown) in Siberia also lead to decreased evaporation (about 0.4 $kg.m^{-2}s^{-1}$; not shown), because more energy is needed to sublimate snow than to evaporate liquid water. Over the Sahel, less MSE is brought from the tropical Atlantic resulting in decreased evaporation and cloud water (Fig. 4, lower left). In the equatorial Atlantic and Pacific Oceans, changes in cloud water and CRF are associated with a different sampling of ENSO signals in the two ten-year averages.

5. Conclusion

A THC collapse simulated in the ECHAM5/MPI-OM climate model induces a dipole pattern in surface temperature, with strong cooling in the Northern Hemisphere and lesser warming in the Southern Hemisphere, resulting in a global surface cooling of 0.72 K. Evidence of a similar pattern has been found in paleodata. It has been associated with a reduction of the northward OHT by the THC, driven by freshwater sources in the Northern Hemisphere (*Bond et al.*, 1992; *Blunier and Brook*, 2001). The mechanisms responsible for the global surface cooling in the ECHAM5/MPI-OM climate model were investigated from a global energy budget point of view. We have shown that fast atmospheric feedbacks are essential to maintain and enhance the global surface cooling due to a THC collapse, as well as for explaining the strong asymmetry in the dipole pattern with Northern Hemisphere anomalies being much larger than opposite Southern Hemisphere anomalies.

The primary ocean-driven surface cooling in the Northern Hemisphere leads to decreased water vapor in the atmosphere. Reduced surface downward long wave radiation results from decreased water vapor and GHG trapping. The increased albedo leads to increased surface upward short wave radiation which acts to cool the surface at high latitudes, but this mechanism is too weak to cause the global surface cooling. Reduced water vapor and increased albedo are necessary to account for the global surface cooling, and the inclusion of both effects can explain the simulated surface cooling in a one-dimensional radiative convective model. The effect of water vapor reduction, however, is much larger than the effect of albedo increase. The water vapor feedback is responsible for maintaining and strengthening the global surface cooling caused by a THC collapse. On the regional scale, changes in cloud water and cloud radiative forcing further modify the surface cooling. A slower ice/albedo feedback and changes in CO_2 concentration may further enhance the global surface cooling on a longer timescale. Asymmetries in time-scale and amplitude between Northern and Southern Hemispheres can thus be understood from the fast atmospheric water vapor response described in this paper.

Aknowledgments. This work was granted by the Dutch Ministry of Transport, Public Works and Water Management. The ESSENCE project, lead by Wilco Hazeleger (KNMI) and Henk Dijkstra (UU/IMAU), was carried out with support of DEISA, HLRS, SARA, and NCF (through NCF projects NRG-2006.06, CAVE-60-023 and SG-06-267). We thank the DEISA Consortium (co-funded by the EU, FP6 projects 508830/031513) for support within the DEISA Extreme Computing Initiative (www.deisa.org). The authors thank Andreas Sterl and Camiel Severijns (KNMI), and HLRS and SARA staff for technical support. Valuable comments from an anonymous reviewer helped improving the manuscript.

References

Blunier, T., and E.J. Brook (2001), Timing of Millennial-Scale Climate Change in Antarctica and Greenland During the Last Glacial Period, *Science*, *291*, 109-112, doi:10.1126/science.291.5501.109.

Bond, G., H. Heinrich, W. Broecker, L. Labeyrie, J. McManus, J. Andrews, S. Huon, R. Jantschik, S. Clasen, C. Simet, K. Tedesco, M. Klas, G. Bonani, and S. Ivy (1992), Evidence for massive discharges of icebergs into the North Atlantic ocean during the last glacial period, *Nature*, *360*, 245-249.

Cheng, W., C.M. Bitz, and J.C.H. Chiang (2007), Adjustment of the Global Climate to an Abrupt Slowdown of the Atlantic Meridional Overturning Circulation, *Geophys. Monogr.*, 19*73*, 295-314.

Laurian, A., S.S. Drijfhout, W. Hazeleger, and B. van den Hurk (2009), Response of the western European climate to a collapse of the thermohaline circulation, *Clim. Dyn.*, doi:10.1007/s00382-008-0513-4.

Manabe, S., and R.F. Strickler (1964), Thermal Equilibrium of the Atmosphere with a Convective Adjustment, *J. Atmosph. Sciences*, *21*, 361-385.

-------------, and R.T. Wetherald (1967), Thermal Equilibrium of the Atmosphere with a Given Distribution of Relative Humidity, *J. Atmosph. Sciences*, *24*, 241-259.

Marsland, S.J., H. Haak, J.H. Jungclaus, M. Latif, and F. Röske (2003), The Max-Planck-Institute global ocean/sea ice model with orthogonal curvilinear coordinates, *Ocean Model*. *5*, 91-127.

Roeckner, E., G. Bäuml, L. Bonaventura, R. Brokopf, M. Esch, M. Giorgetta, S. Hagemann, I. Kirchner, L. Kornblueh, E. Manzini, A. Rhodin, U. Schlese, U. Schulzweida, and A. Tompkins (2003), The atmospheric general circulation model ECHAM 5. Part I: Model description. Tech. Rep. 349, Max-Planck-Institut für Meteorologie, Hamburg, Germany.

Sterl, A., C. Severijns, H. Dijkstra, W. Hazeleger, G.J. van Oldenborgh, M. van den Broeke, G. Burgers, B. van den Hurk, P.J. van Leeuwen, and P. van Velthoven (2008), When can we expect extremely high surface temperature? *Geophys. Res. Lett.*, *35*, L14703, doi:10.1029/2008GL034071.

Stouffer, R.J., J. Yin, J.M. Gregory, K.W. Dixon, M.J. Spelman, W. Hurlin, A.J. Weaver, M. Eby, G.M. Flato, H. Hasumi, A. Hu, J.H. Jungclaus, I.V. Kamenkovich, A. Levermann, M. Montoya, S. Murakami, S. Nawrath, A. Oka, W.R. Peltier, D.Y. Robitaille, A. Sokolov, G. Vettoretti, S.L. Weber (2006), Investigating the Causes of the Response of the Thermohaline Circulation to Past and Future Climate Changes, *J. Clim.*, *19*, 1365-1387.

Van Dorland, R. (1999), Radiation and Climate From Radiative Transfer Modelling to Global Temperature Response. Ph.D. thesis, Utrecht University, The Netherlands, 147 pp. ISBN 90-646-4032-7.

Vellinga, M., and R.A. Wood (2002), Global climatic impacts of a collapse of the Atlantic thermohaline circulation, *Clim. Change*, 54, 251-267, doi: 10.1023/A:1016168827653.

---------------, and P. Wu (2008), Relations between Northward Ocean and Atmosphere Energy Transports in a Coupled Climate Model, *J. Clim. 21*, 561-575.

List of tables

Table 1. Sensitivity experiments performed with the RCM. The first line gives the anomalous surface temperature (K) and water vapor (q; $g.kg^{-1}$) in the climate model (H-E stands for HOSING-ENSMALL). Cloud stands for cloud cover, RH stands for relative humidity, and Fb for water vapor feedback. Pr stands for prescribed: the value or profile is fixed with a prescribed anomaly due to a THC collapse. Fx stands for fixed: the value is fixed to the RCM reference value. Adj stands for adjusted: the profile is free to adjust. The anomalous surface temperature and water vapor (noted dT and dq), computed as the difference between a given experiment and the reference run, are also shown.

Name of experiment	Albedo	Cloud	q	RH	Fb	dT	dq
H-E	--------	--------	------	------	-------	-0.72	-0.33
Ref	Fx	Fx	Fx	Fx	-------	0	0
Alb_NoFb	Pr	Fx	Fx	Adj	off	-0.08	0
Alb_Fb	Pr	Fx	Adj	Fx	on	-0.15	-0.08
q_NoFb	Fx	Fx	Pr	Adj	off	-0.53	-0.33
Alb-q_NoFb	Pr	Fx	Pr	Adj	off	-0.62	-0.33
Cld_Fb	Fx	Pr	Adj	Fx	on	-0.01	0
Cld-Alb-q_NoFb	Pr	Pr	Pr	Adj	off	-0.62	-0.33

Figure captions

Fig. 1. Left: annual change in two-meter air temperature computed as the difference between HOSING and ENSMALL (K). Right: globally averaged annual change in two-meter air temperature (K).

Fig. 2. Left: Annual mean surface radiation budget ($W.m^{-2}$) in ENSMALL (orange) and HOSING (purple) over the period 2091-2100. Right: Same for the difference between HOSING and ENSMALL.

Fig. 3. Annual change in LH (upper left), surface downward LW (upper right), upward SW (lower left), and downward SW (lower right), computed as the difference between HOSING and ENSMALL. Note the different color scales ($W.m^{-2}$).

Fig. 4. Upper left: annual mean change in surface specific humidity ($g.kg^{-1}$) computed as the difference between HOSING and ENSMALL. Upper right: same for the column-integrated moist static energy ($km^3 s^{-2}$). Lower left: annual mean change in column-integrated cloud water ($g.m^{-2}$). Lower right: annual mean change in cloud radiative forcing, computed as the difference between the radiative fluxes at the top of the atmosphere with clouds and under clear-sky conditions ($W.m^{-2}$).

List of figures

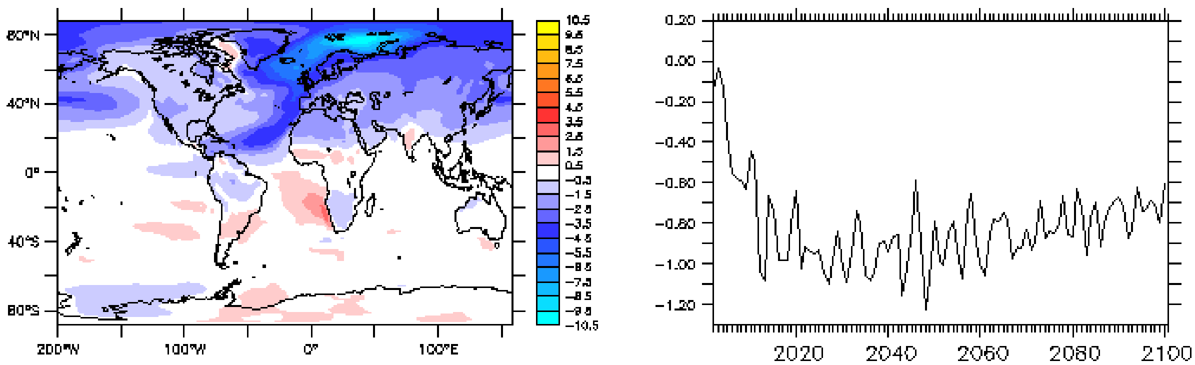

Fig. 1. Left: annual change in two-meter air temperature computed as the difference between HOSING and ENSMALL (K). Right: globally averaged annual change in two-meter air temperature (K).

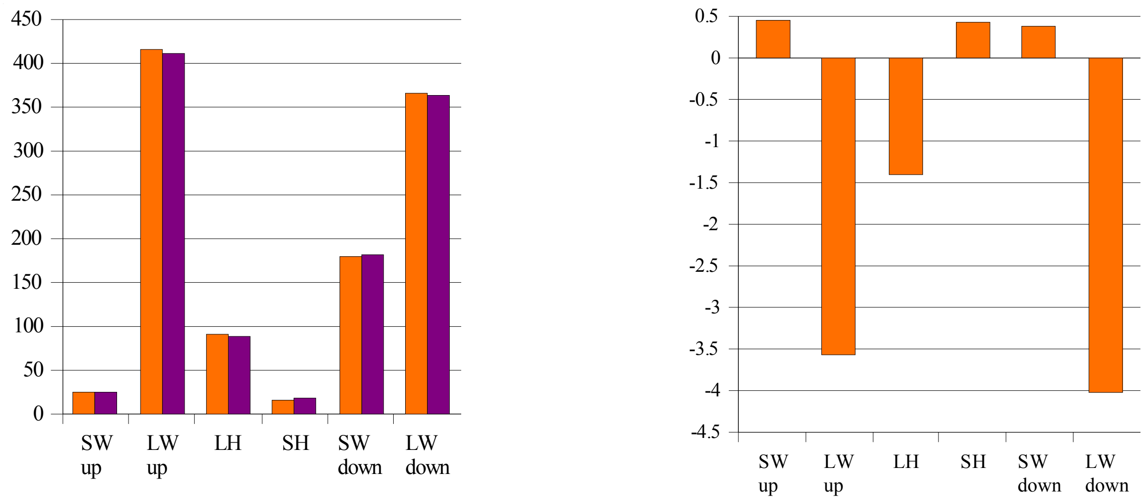

Fig. 2. Left: Annual mean surface radiation budget ($W.m^{-2}$) in ENSMALL (orange) and HOSING (purple) over the period 2091-2100. Right: Same for the difference between HOSING and ENSMALL.

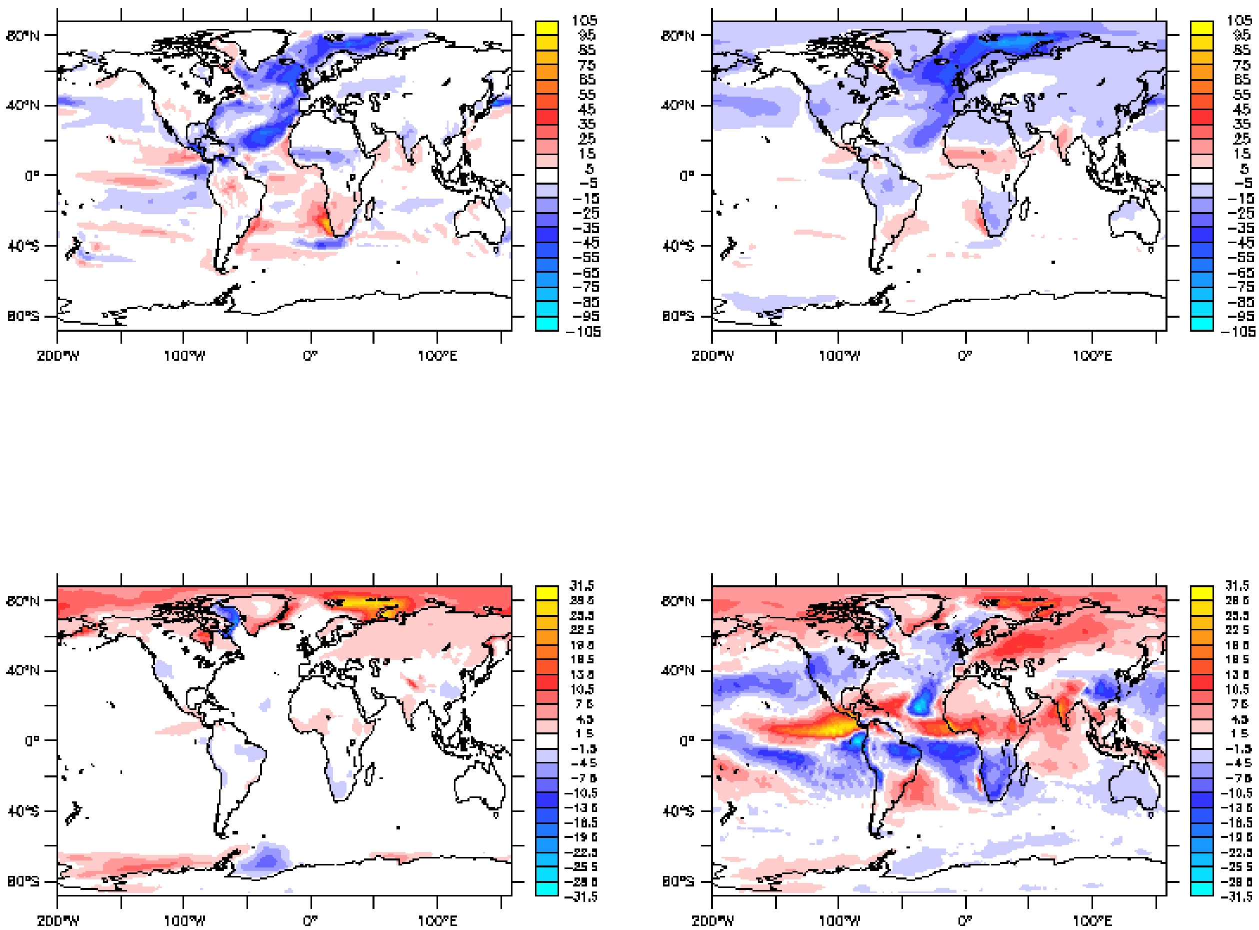

Fig. 3. Annual change in LH (upper left), surface downward LW (upper right), upward SW (lower left), and downward SW (lower right), computed as the difference between HOSING and ENSMALL. Note the different color scales ($W.m^{-2}$).

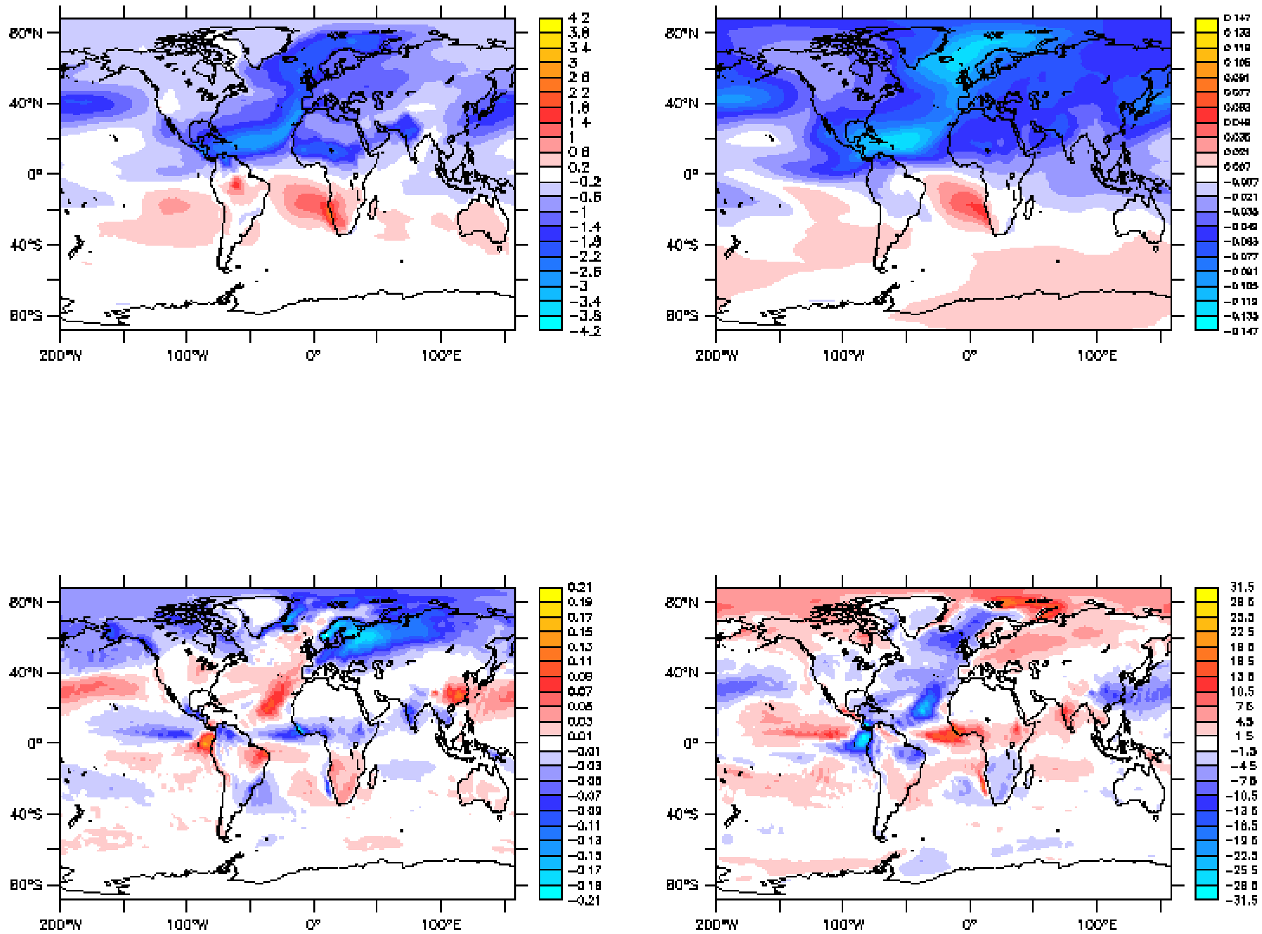

Fig. 4. Upper left: annual mean change in surface specific humidity ($g.kg^{-1}$) computed as the difference between HOSING and ENSMALL. Upper right: same for the column-integrated moist static energy ($km^3 s^{-2}$). Lower left: annual mean change in column-integrated cloud water ($g.m^{-2}$). Lower right: annual mean change in cloud radiative forcing, computed as the difference between the radiative fluxes at the top of the atmosphere with clouds and under clear-sky conditions ($W.m^{-2}$).